Expanding quasiperiodicity in soft matter: Supramolecular decagonal quasicrystals by binary giant molecule blends

Yuchu Liu[a,b,1], Tong Liu[a,b,1], Xiao-Yun Yan[a,b], Qing-Yun Guo[a,b], Huanyu Lei[a], Zongwu Huang[a], Rui Zhang[a], Yu Wang[a,c], Jing Wang[a], Feng Liu[d], Feng-Gang Bian[e], E.W. Meijer[f], Takuzo Aida[g,h], Mingjun Huang[a,c,2], and Stephen Z.D. Cheng[a,b,2]

[a]South China Advanced Institute for Soft Matter Science and Technology, School of Molecular Science and Engineering, South China University of Technology, Guangzhou 510640, China; [b]Department of Polymer Science, School of Polymer Science and Polymer Engineering, University of Akron, Akron, OH 44325; [c]Guangdong Provincial Key Laboratory of Functional and Intelligent Hybrid Materials and Devices, South China University of Technology, Guangzhou 510640, China; [d]State Key Laboratory for Mechanical Behaviour of Materials, Shaanxi International Research Center for Soft Matter, Xi'an Jiaotong University, Xi'an 710049, China; [e]Shanghai Synchrotron Radiation Facility, Shanghai Advanced Research Institute, Chinese Academy of Sciences, Shanghai 201210, China; [f]Laboratory of Macromolecular and Organic Chemistry, Institute for Complex Molecular Systems, Eindhoven University of Technology, 5600 MB Eindhoven, The Netherlands; [g]Department of Chemistry and Biotechnology, School of Engineering, The University of Tokyo, Tokyo 113-8656, Japan; and [h]Riken Center for Emergent Matter Science, Wako 351-0198, Japan

Edited by Frank Bates, Chemical Engineering and Materials Science, University of Minnesota, Minneapolis, MN; received August 19, 2021; accepted November 25, 2021

The quasiperiodic structures in metal alloys have been known to depend on the existence of icosahedral order in the melt. Among different phases observed in intermetallics, decagonal quasicrystal (DQC) structures have been identified in many glass-forming alloys yet remain inaccessible in bulk-state condensed soft matters. Via annealing the mixture of two giant molecules, the binary system assemblies into an axial DQC superlattice, which is identified comprehensively with meso-atomic accuracy. Analysis indicates that the DQC superlattice is composed of mesoatoms with an unusually broad volume distribution. The interplays of submesoatomic (molecular) and mesoatomic (supramolecular) local packings are found to play a crucial role in not only the formation of the metastable DQC superlattice but also its transition to dodecagonal quasicrystal and Frank–Kasper σ superlattices.

soft matter | hierarchical self-assembly | phase transition | decagonal quasicrystalline

Quasicrystals (QCs) are crystals with "forbidden" rotational symmetry (i.e., 5-, 8-, 10-, 12-fold, etc.) and "quasiperiodic" translational symmetry (1). Soon after the first discovery of the 10-fold Al-Mn QC by Shechtman et al. in 1984 (2), various QC alloys have been successively identified (3, 4), and among them are three-dimensional (3D) icosahedral QCs (IQC) (5–10), 10-fold two-dimensional (2D) decagonal QCs (DQC) (11–14), and 12-fold 2D dodecagonal QCs (DDQC) (15, 16). Recently, various condensed soft matters [e.g., block copolymers (17–21), dendrimers (22, 23), and giant molecules (24–26)] were also reported to form supramolecular DDQCs by a hierarchical assembling procedure. In these cases, the submesoatomic (molecular) units first aggregate into mesoatoms (i.e., the supramolecular spherical motifs compared to "atoms" in the metal alloy crystals), and then, the mesoatoms further assemble into the quasicrystalline superlattices (QC-SLs).

Apart from the stable QCs with fine-tune composition and conditions (27), metallic QCs often arise from either the rapid cooling of the melted alloys or the partial devitrifications of the metallic glasses (3, 28), and these QC alloys are generally reckoned metastable. In these structures, frustrated clusters of icosahedral order widely exist (29) because of the most efficient local tetrahedral packing as suggested by Frank (30). Correspondingly, the formation of soft QC-SLs suggests similar clusters also exist on the mesoatomic level (among mesoatoms) (31). Interestingly, while most metallic QC alloys are IQC or DQC, the 12-fold DDQCs are rare for metals. On the contrary for condensed soft matters, though 10-fold QC and 18-fold QC have been occasionally reported in colloidal thin film and colloidal micelles (32, 33), most QC-SLs found in bulk state adopt 12-fold DDQC structure. While the formation of the various complex intermetallic structures—by atoms in alloys and mesoatoms in soft matter—reinforces the scale-invariance principle, the formation of different QC structures in metallic alloys and condensed soft matters hints a hidden complexity in packing behaviors at different scales.

Previously, we reported a unique self-assembling strategy for binary blends of giant molecules (34). Mediated by a self-sorting mechanism, two mixed giant molecules with identical corona but different core structures can aggregate in a self-recognized manner, forming two specific mesoatomic species of

Significance

As the formation of quasicrystalline ordering in both metal alloys and soft matters reinforces the scale-invariance principle, however, it remains unknown that why metallic quasicrystals prefer decagonal quasicrystalline (DQC, 10-fold) ordering, and the condensed soft maters only exhibit dodecagonal quasicrystalline (DDQC, 12-fold) ordering. By tuning the self-sorting ability in a pair of giant molecules, the well-mixed binary blends generate a metastable DQC phase and corresponding unprecedent phase sequence (DQC → DDQC → Frank–Kasper σ) during thermal annealing. These peculiar assembling behaviors result from interplays of submesoatomic and mesoatomic packings. Reducing the self-sorting strength has induced an extra complexity in the submesoatomic packings of giant molecules, which further influences the clustering on the mesoatomic level.

Author contributions: Y.L., T.L., M.H., and S.Z.D.C. designed research; Y.L., T.L., X.-Y.Y., Q.-Y.G., H.L., Z.H., and R.Z. performed research; Y.L., T.L., X.-Y.Y., Q.-Y.G., H.L., J.W., F.L., F.-G.B., and S.Z.D.C. contributed new reagents/analytic tools; Y.L., T.L., H.L., Z.H., R.Z., Y.W., J.W., M.H., and S.Z.D.C. analyzed data; and Y.L., T.L., E.W.M., T.A., M.H., and S.Z.D.C. wrote the paper.

The authors declare no competing interest.

This article is a PNAS Direct Submission.

[1]Y.L. and T.L. contributed equally to this work.

[2]To whom correspondence may be addressed. Email: huangmj25@scut.edu.cn or scheng@uakron.edu.

This article contains supporting information online at http://www.pnas.org/lookup/suppl/doi:10.1073/pnas.2115304119/-/DCSupplemental.

Published January 12, 2022.

discrete sizes. Depending on the radius ratio of the mesoatom pair, these binary mixtures replicate the metallurgy of MgZn and MgCu alloys. However, at the eutectic composition (i.e., the marginal composition between the intermetallic phase and the primary phase), besides the decomposition into two phases, a peculiar formation of DDQC-SLs was identified. Accordingly, the DDQC-SLs are only formed by mesoatoms with much smaller radius ratio (31, 35), which suggests the failure of self-sorting behavior in this special case. Such failure could be due to the partial miscibility among different giant molecules and enable the formation of various hybrid mesoatomic species, adding another degree of complexity for packings on the submesoatomic level. This observation sparked the interesting question whether further reducing the self-sorting strength can indeed complicate the packings on a submesoatomic level, and if so, can this additional complexity trigger more interesting assembling behaviors on the mesoatomic level, leading the formation of unexplored complex structures in condensed soft matters.

Results and Analysis

To tackle this challenge, we designed a pair of multibranched giant molecules—**OP8** and **OP14** (Fig. 1*A*)—by tethering eight and 14 aliphatic isooctyl-polyhedral oligomeric silsesquioxane (OPOSS) cages, respectively, to the core multifunctionalized POSS. The final step in the synthesis was the coupling the core and the cages via the copper-catalyzed azide–alkyne [3 + 2] cycloaddition. Differing from the previously reported binary systems (34), these two giant molecules have similar chemical structures in both the core and periphery groups, and only the numbers of periphery OPOSS cages vary. Upon annealing, self-aggregation will take place, forming mesoatoms with aliphatic OPOSS cages located at periphery and aromatic linkers at the core. Annealed separately, **OP8** and **OP14** self-assemble into the Frank–Kasper σ (FK σ, $P4_2/mnm$) phase of different sizes. **OP8** has a lattice with $\boldsymbol{a}$ = 22.4 nm, $\boldsymbol{c}$ = 11.8 nm, and by mesoatoms with average radius r_1 = 3.70 nm (Fig. 1*B*). **OP14** possesses a lattice with $\boldsymbol{a}$ = 18.9 nm, $\boldsymbol{c}$ = 9.93 nm, and by mesoatoms with average radius r_2 = 3.03 nm (Fig. 1*C*). These detailed mesoatom structures were further analyzed by molecular dynamic simulation (details in *SI Appendix*). Interestingly, though **OP8** and **OP14** have similar chemical structures and molecular radii, they aggregate by different packing modes. **OP8** with fewer branches adopts a double-shell packing (Fig. 1*B*), inserting several OPOSS cages into the core of the mesoatoms. In contrast, **OP14** with more branches can only aggregate into the smaller single-shell mesoatoms (Fig. 1*C*). The completely different packing mode of **OP8** and **OP14** drives us to explore the self-assembly behavior in their binary blends and particularly the volume distribution of the resultant mesoatoms.

We prepared freeze-dried **OP8/OP14** binary mixtures of different compositions, annealed them, and probed these mixtures in situ by synchrotron small-angle X-ray scattering (SAXS, detailed sample preparations and characterizations, see *Materials and Methods*). During heating, a special phase transition behavior was captured for the blend **OP8/OP14** at mass ratio = 1:2. This specimen exhibits an unknown SAXS pattern at 120 °C (red solid curve in Fig. 2*E*) with two previously identified DDQC-SL and FK σ structure at higher temperatures following a phase sequence of the unknown phase → DDQC →FK σ (Fig. 2*E*). With different compositions, a structure diagram (Fig. 1*D*) has been obtained by probing the assembling structures in situ during heating, and the unknown phase is shown in red area. In the following analysis and further discussions, we focus on the blend of **OP8/OP14** at mass ratio = 1:2 to study this unknown structure and refer to this blend as "the sample" if not otherwise specified.

Transmission electron microscopy (TEM) was conducted to resolve this unknown structure (see *Materials and Methods* and *SI Appendix*). Fig. 3*A* shows a unique pattern that demonstrates an overall 10-fold rotational symmetry as indicated by fast Fourier transform (FFT) results and Fourier filtered patterns (Fig. 3 *B* and *C*). These results suggest the quasiperiodicity on the TEM imaging plane (we here defined as the *x-y* plane). Detailed tiling features were further analyzed with the raw TEM image (Fig. 3*D*). First, the mesoatoms' positions were assigned to the centers of each dark spots (red dots in Fig. 3*D*). Then, the Delaunay triangulation was performed based on mesoatoms' position, presenting the connecting vectors of each pairs of neighboring mesoatoms (partially presented in Fig. 3*D* and *SI Appendix*, Fig. S9). Finally, these vectors were further summarized as a density heat map present in Fig. 3 *E* and *F*. Three sets of characteristic vectors (i.e., $\boldsymbol{a}$, $\boldsymbol{b}$, and $\boldsymbol{c}$ as indicated in Fig. 3*E*) distribute evenly with 2π/10 angular intervals, validating the overall 10-fold symmetry. If only delineating the major characteristic vector $\boldsymbol{a}$, the quasiperiodic patterns are

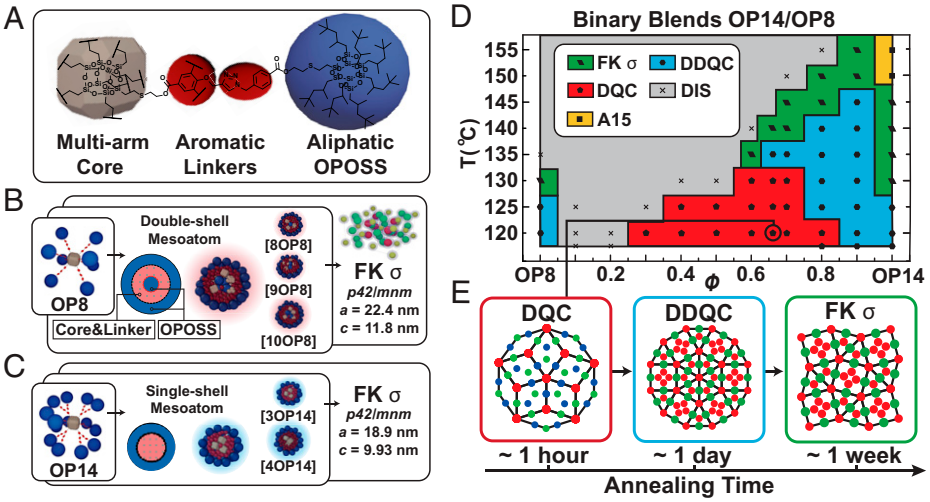

Fig. 1. Self-assembling of giant molecule **OP8**, **OP14**, and their binary blends **OP8/OP14**. (*A*) Chemical structures and molecular components of **OP8** and **OP14**. (*B*) Molecular model of **OP8** and its hierarchical self-assembling procedure to FK σ superlattice. (*C*) Molecular model of **OP14** and its hierarchical self-assembling procedure to FK σ superlattice. (*D*) Composition temperature structure diagram of binary blends **OP8/OP14** probed by in situ SAXS during the first heating (note: the phase diagram for the final structures after ex situ long-time annealing is shown in *SI Appendix*, Fig. S7). (*E*) DQC → DDQC → FK σ structure evolution of the binary blends **OP8/OP14** of mass ratio = 1:2 at 120 °C.

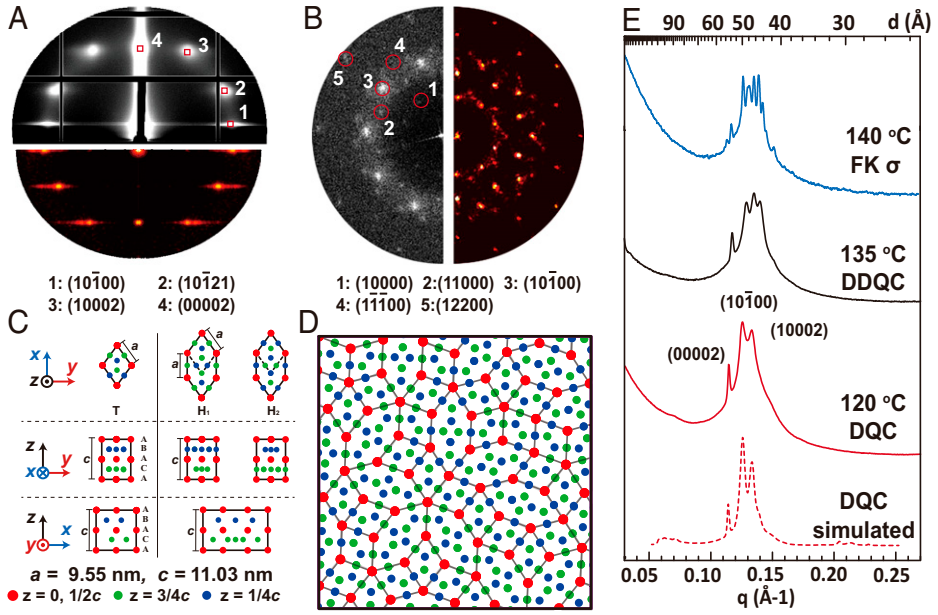

Fig. 2. Characterizations of DQC-SL. (*A*, *Upper*) Experimental GISAXS pattern. (*Bottom*) Simulated GISAXS pattern. (*B*, *Left*) The FFT pattern of experimental quasiperiodic plane as in Fig. 3*B*. (*Right*) Simulated result. (*C*) Proposed mesoatomic decoration in tiling units. (*D*) Reconstructed DQC-SL based on the Mg-Zn-Y four-layer DQC model. (*E*) Experimental SAXS result of the binary assemblies at different temperatures and simulated DQC SAXS result.

reckoned as a tessellation of fat rhombus and flattened hexagons (Fig. 3*A*). While the major featuring length $\boldsymbol{a}$ = 8.7 nm characterize the side length of the tiles, the other two lengths $\boldsymbol{b}$ = 10.3 nm (2sin(π/5) × $\boldsymbol{a}$) and $\boldsymbol{c}$ = 13.5 nm (($\boldsymbol{a}^2 + \boldsymbol{b}^2$)$^{1/2}$) represent the other two characteristic lengths in these two tiles (Fig. 3 *A*, *Inset*). Interestingly, such tessellations highly resemble the axial DQC observed in Mg-Zn-Y alloys (36–38).

To probe its axial periodicity (*z* directions, perpendicular to the *x*-*y* plane), grazing incident small-angle X-ray scattering (GISAXS) was applied on the spin-coated thin film samples. The sample annealed at 120 °C affords a GISAXS pattern (Fig. 2 *A*, *Upper*) of three major features: 1) three sets of diffractions peaks are separated by an identical vertical interval Δq_z ~0.056 Å^{-1}; 2) the axial diffraction q_z ~$2\Delta q_z$ coincides with the front peak in SAXS of the unknown structure, and it also matches the {00002} peak of DDQC and {002} peak of FK σ along the phase transition; and 3) the diffraction peak of {00001} is extinct (corresponding to the peak at $q_{xy} = 0$, $q_z = \Delta q_z$), suggesting a symmetric electron density distribution at both sides of z = 1/2$\boldsymbol{c}$ planes, which is also the case with the later emerging DDQC and FK σ phases. These observations suggest the axial arrangement of the unknown structures is highly related to the DDQC and FK σ phase, which also agrees well with the Mg-Zn-Y–type axial DQC (36–38).

Based on the Mg-Zn-Y DQC model, an ABAC-type mesoatomic decoration was assigned to the rhombic and flat hexagon QC structural unit as presented in Fig. 2*C*. A super unicell containing 5,000+ mesoatoms was reconstructed following the tiling rules (partially shown in Fig. 2*D* and *SI Appendix*, Fig. S10). Direct 3D Fourier transformations were applied to simulate the structure's diffractions in 3D reciprocal space. Different integration processes were then adopted to afford the simulated GISAXS and TEM FFT results (Fig. 2 *A* and *B*, and for details, see *SI Appendix*). The SAXS result was otherwise simulated by specialized powder diffraction simulation programs (Fig. 2*E*, for details, see *SI Appendix*). The simulated and experimental diffractions can be properly assigned according to axial DQC model, and these simulated results agree well with experimental data (Fig. 2 *A*, *B*, and E). These results prove the unknown structure adopts an Mg-Zn-Y–type four-layer DQC-SL.

The phase sequence was further investigated to reveal the thermodynamic property of the associated phases. At 120 °C, the SAXS pattern of DQC has been well developed (Fig. 2*E*). Raising the temperature to 135 °C, a SAXS pattern of DDQC was recorded. Carefully increasing the temperature to 140 °C results in a distinctive scattering pattern of an FK σ phase following a sequence of DQC → DDQC → FK σ. The specimen reached a disordered state above 145 °C. The sample retained disorder cooling from 160 °C to room temperature at the rate of −30 °C/min, and the same phase sequence recurs upon reheating. In addition, when annealed for 1 wk at 120 °C, the DQC gradually evolves into the FK σ phase (Fig. 1*E* and *SI Appendix*, Fig. S8). The phase sequence of DQC → DDQC → FK σ during the heating or long-time annealing demonstrates a unique transition of two metastable QC states, which is rarely seen.

Discussion

To further investigate the packing details, we reconstruct the Wigner–Seitz (WS) cells for each assembled structure (FK σ by unblended **OP8** and unblended **OP14**; DQC, DDQC, and FK σ by **OP8**/**OP14** at mass ratio = 1:2.). The WS cells can well approximate the sizes and shapes of the mesoatoms in their associated SL (Fig. 4 *B*–*E*). Further aided by molecular dynamic (MD) simulations (for details, see *SI Appendix*), these cells provide valuable insights for the mesoatom formation in various supramolecular structures.

By this method, we first study the mesoatoms in two unblended assemblies (FK σ by **OP8** and **OP14**, individually), and two packing modes were identified. The FK σ structure by **OP14** contains WS cells with volumes in between mesoatoms **[3OP14]** and **[4OP14]** (Figs. 1*C* and 4 *B*, *Left*), both adopting a single-shell packing mode (i.e., aromatic linkers aggregate inside forming the core, while all aliphatic OPOSS are purged outside forming the shell). The FK σ superlattice of **OP8** contains WS cells having similar volumes with mesoatoms **[8OP8]**

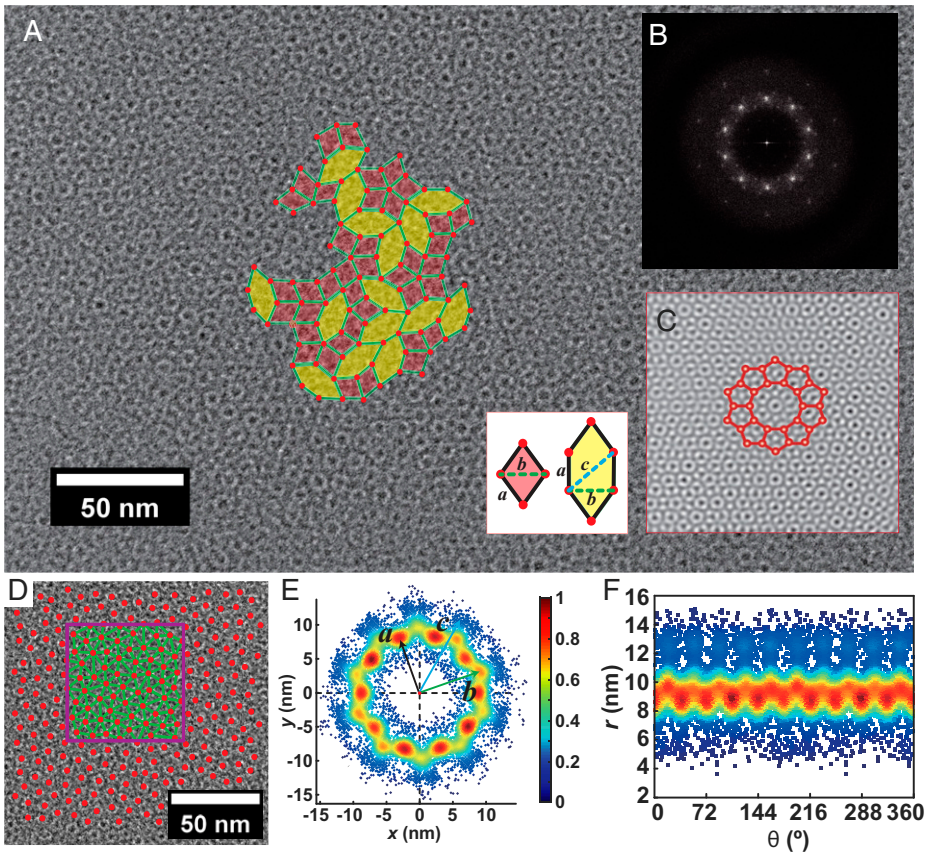

Fig. 3. DQC-SL TEM structural analysis. (*A*) RuO_4-stained TEM image of binary blends **OP8/OP14** = 1/2 annealed at 120 °C. (*Inset*) Two tiling elements of fat rhombus and hexagons. (*B*) FFT results. (*C*) Fourier-filtered TEM result. (*D*) Example of TEM image processing: 1) Extracting mesoatoms positions marked (red dots). 2) Calculating the connecting vectors (green lines) by the Delaunay triangulation. (*E*) Density heatmap of the connecting vector distribution in *x-y* coordination and in (*F*) r-θ coordination.

to **[10OP8]** (Figs. 1*B* and 4 *B*, *Right*). Differed from the single-shell **OP14** mesoatoms, the less branched **OP8** giant molecules can aggregate via a double-shell mode since the single-shell mode for more crowded **OP14** suffers great entropic penalty, leaving a few aliphatic OPOSS in the center of the aromatic core as indicated by MD simulation (*SI Appendix*, Fig. S13). This double-shell packing increases the radius of the mesoatoms and lowers the overall surface volume ratio (for detailed calculations, see *SI Appendix*) to reduce its overall free energy.

For the binary assemblies, since the chemical structures of **OP8** and **OP14** are highly alike, **OP8** and **OP14** tend to mix to a certain degree during their aggregation into mesoatoms. Then the hybrid mesoatoms **[*x*OP8/*y*OP14]** of various sizes will be formed via either single-shell or double-shell packing modes, depending on the detailed hybrid composition. By simulating the stable packing models of mesoatoms **[*x*OP8]** and **[*y*OP14]** at different compositions (Fig. 4*A* and *SI Appendix*, Fig. S13), we identified three mesoatomic volume zones, favoring the single-shell, transitional, and double-shell packing methods (as colored by blue, white, and red zones in Fig. 4 *B*–*E*, respectively). Within this frame, the mesoatomic compositions in the blending assemblies are further studied: the DQC-SLs demonstrate an unusually wide volume distribution (Fig. 4*C*) containing both single-shell and double-shell mesoatoms. Moreover, this distribution only overlaps slightly with the unblended **OP8** and **OP14** FK σ assemblies (Fig. 4*B*), suggesting the minority of discrete single component **[*x*OP8]** or **[*y*OP14]** mesoatoms and the majority of hybrid mesoatom **[*x*OP8/*y*OP14]** compositions. Meanwhile, these hybrid **[*x*OP8/*y*OP14]** mesoatoms also possess a volume polydispersity of which is bounded by the volumes between aforementioned single-shell and double-shell mesoatoms. This set of mesoatoms finally constructs the DQC-SL; as it later transforms into the DDQC-SL, the majority of double-shell mesoatoms diminishes, affording the DDQC structure with a narrower mesoatomic volume distribution (Fig. 4*D*). As the structure evolves into the final stable FK σ phase, the distribution further unifies (Fig. 4*E*).

As the emergence of QC ordering suggest the existence of nonequilibrium but kinetically facilitated particles clustering in both condensed soft matters (31) and metallic alloys (29, 39), additional kinetically favored packing from the submesoatomic level has been spotted in our case—namely, those later-diminished larger double-shell mesoatoms. Furthermore, according to the valuable insights from other soft matter systems, the interplays of local packings on both submesoatomic and mesoatomic level are critical for these intriguing assembling behaviors in our case (Fig. 4*F*): 1) Starting from the amorphous binary blends, the local configurations of the mixed giant molecules will transit to either single-shell or double-shell mesoatoms upon annealing. 2) Though the double-shell mesoatoms are in a nonequilibrium state, for certain local configurations, they are kinetically more favored within the reach of minimum rearrangement (40). Thus, these double-shell mesoatoms form once annealed at low temperature and persist because of the limited diffusion of the giant molecules (41, 42). 3) With the emergence of mesoatoms of such broad volume distribution, the DQC lattice with 10-fold symmetry becomes the optimized structure to include all the mesoatoms via tetragonally close packing with minimum rearrangement. 4) When annealed for a longer time or at higher temperature, giant molecules within double-shell mesoatoms gradually redistribute, forming smaller

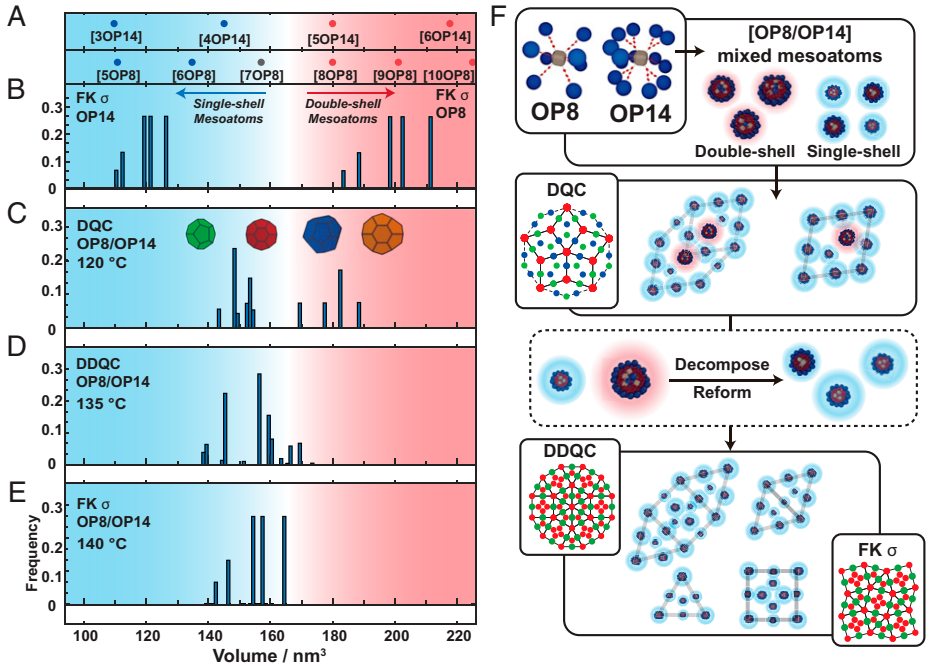

Fig. 4. Structural analysis of various SLs. (*A*) Calculated volumes and the stable packing models of unblended mesoatoms **[*x*OP8]** and **[*y*OP14]**. (*B*) The volume distribution of reconstructed WS cells for FK σ by pure **OP14** (*Left*) and pure **OP8** (*Right*). (*C–E*) The WS cells volume distribution of DQC, DDQC, and FK σ assembled by blends of **OP8/OP14** at mass ratio = 1:2. (*F*) Schematic representation of proposed assembling mechanism during the phase transition of DQC → DDQC → FK σ.

but more stable single-shell species (Fig. 4 *F*, *Middle*). This redistribution on a submesoatomic level further change the packings on the mesoatomic level, affording the characteristic "triangle square" tiling elements for DDQC and FK σ structures (23). Inherited from the random tiling in DQC-SLs, the random distribution of these "triangle square" tiling elements leads to a metastable DDQC-SL (20, 43). 5) When annealed for an even longer time, the DDQC structure gradually reforms into its crystalline approximant—the FK σ structures—potentially reaching its global minimum. The details of the redistribution dynamic between single-shell and double-shell mesoatoms remain to be explored.

As for the question why DQC is seldom observed in condensed soft matters and DDQC is rare for metal alloys, we would share some inspiring thoughts based on the deep analysis of the aforementioned DQC system in binary giant molecule blends. The formation of DQC-SLs usually requires a wider volume distribution of the constructing mesoatoms, which is hard to achieve for a "single-component" supramolecular assembly. However, at the atomic scale, similar criterion can be easily fulfilled by multielement metallic alloys (12). Therefore, DQC structures are seldom seen in soft matters but widely exist in alloys. On the contrary, 12-fold DDQC structures possess a relatively narrower volume distribution (nearly identical with FK σ structures). For the metallic atoms, they can easily nucleate into the stable FK σ (or other crystalline approximants) crystals instead of being trapped in metastable DDQC state (16). For supramolecular assemblies in soft matter, since rearranging the mesoatoms needs either higher kinetic energy or longer time, less stable local configurations can preserve at more general conditions (44). Thus, DDQC structures are more frequently observed in condensed soft matters and less in alloys.

Conclusion

The discovery of DQC structures and its intriguing transition (i.e., DQC → DDQC → FK σ) in our binary giant molecule blends is unprecedented. Complex interplays of packings on two hierarchical levels—the submesoatomic level and mesoatomic level—are found to play the central role in the peculiar assembling behaviors. In our case, reducing the self-sorting strength in the binary giant molecule blends has introduced an extra degreed of complexity on submesoatomic packings. The resultant mesoatoms with a broad volume distribution induce unusual local packings on mesoatomic level, affording the DQC-SL. Moreover, with the redistributions of giant molecules, packings on both submesoatomic and mesoatomic level change simultaneously, leading the transitions toward the stable FK σ structure via an intermediate DDQC state. While such interplays might widely exist in various hierarchical assemblies of soft matters, these specifically designed giant molecules have offered us valuable insight to the hidden complexity behind different hierarchical levels.

Materials and Methods

General Methods and Equipment. ^{1}H and ^{13}C experiments were measured on a Varian Mercury 500 M NMR or 300 M NMR spectrometer. Gel permeation chromatography was measured in tetrahydrofuran at 35 °C on Tosoh EcoSEC instrument with three columns (TSKgel SuperH3000 × 2, TSKgel SuperH5000), a Guard Column (TSKgel SuperH1000-4000), and an ultraviolet detector. A JEOL-1230 TEM with an accelerating voltage of 120 kV was utilized to record the bright field images of thin sections of different samples. Fast Fourier transformation results and FFT-filtered images were performed on ImageJ software. The density of the samples was measured by the floatation method. The experimental measured density of these phases formed by the giant shape amphiphiles is $\rho = 1.07$ (g/cm^3). SAXS and GISAXS were collected at beamline BL16B1 of the Shanghai Synchrotron Radiation Facility (SSRF). The one-dimensional circular integrations of 2D SAXS patterns were performed by the Igor Pro-6.37 (with Nika 2D SAS macros) software package. The GISAXS results were analyzed by GIXSGUI (45). As the identical methods and settings were also used in several of our previous reports, more detailed descriptions are documented in ref. 34.

Giant Molecular Monomer Sample Preparation. The detailed synthetic procedures are recorded in detail in *SI Appendix*. All pure giant molecule product was transferred in to separate vials and dried under vacuum before further operation.

Giant Molecular Blends Preparation. Both the pure **OP8** and **OP14** were transferred into separate vials and dried under vacuum before further operation. Equal mass (20 mg) of each giant molecule was separately dissolved in 7.5 mL methylene chloride, and then, the calculated volume of stock solution (for example 100, 200 … 900 μL) was taken and mixed to afford target compositions. The mixtures were dried under vacuum, redissolved in benzene (0.5 mL), and further freeze dried to afford sticky white solids.

SAXS sample. A small piece of blended sample was placed into an aluminum sample holder and sealed by the Kapton tape. For ex situ SAXS, a Mettler Toledo FPHT hot stage was used for sample annealing. All thermal annealing process were performed under the nitrogen atmosphere. The samples of different blending mass ratios were annealed at target temperatures for 12 h, and at least three pieces of samples were annealed at the same time to confirm reproducibility. The in situ SAXS results were obtained by annealing the specimen in line at different temperatures. At each targeted temperature, the specimen was measured at least three times with 5-min intervals until no change was detected in diffraction patterns.

TEM Sample Preparation. The samples for TEM experiments were prepared by dropping 5 μL sample solution (1 mg/mL in dichloromethane) onto carbon-coated copper grids. After the solvent evaporation, the copper grids were annealed at 120 °C for 3 h, then cooled down to room temperature. The annealed samples were further stained by RuO_4.

GISAXS Sample Preparation and Characterization. The samples for GISAXS experiments were prepared by spin coating the sample solution (10 mg/mL in dichloromethane) onto a clean silicon wafer. After the solvent evaporation, the specimen was then annealed at 120 °C for 3 h, then cooled down to room temperature. The annealed samples were directly characterized by GISAXS.

Data Availability. SAXS, GISAXS, TEM and diffraction simulation data are publicly available at http://dx.doi.org/10.17605/OSF.IO/ES43X.

All other study data are included in the article and/or *SI Appendix*.

ACKNOWLEDGMENTS. We thank the staff of Beamline BL16B1 at the SSRF for assistance with the SAXS experiments. This work is supported by NSF (DMR-1408872 to S.Z.D.C.), the National Natural Science Foundation of China (U1832220 to S.Z.D.C.), the Guangdong Provincial Key Laboratory of Functional and Intelligent Hybrid Materials and Devices (no. 2019B121203003), the Recruitment Program of Guangdong (no. 2016ZT06C322), Major Program of National Natural Science Foundation of China (no. 51890871), and the Fundamental Research Funds for the Central Universities (no. 2019JQ05 to M.H.).

1. D. Levine, P. J. Steinhardt, Quasicrystals. I. Definition and structure. *Phys. Rev. B Condens. Matter* **34**, 596–616 (1986).
2. D. Shechtman, I. Blech, D. Gratias, J. W. Cahn, Metallic phase with long-range orientational order and no translational symmetry. *Phys. Rev. Lett.* **53**, 1951–1953 (1984).
3. A. P. Tsai, *Physical Properties of Quasicrystals*, Z. M. Stadnik, Ed. (Springer, Berlin, Heidelberg, **vol. 1984**, 1999), pp. 5–50.
4. W. Steurer, Quasicrystals: What do we know? What do we want to know? What can we know? *Acta Crystallogr. A Found. Adv.* **74**, 1–11 (2018).
5. P. A. Heiney *et al.*, Disorder in Al-Li-Cu and Al-Mn-Si icosahedral alloys. *Science* **238**, 660–663 (1987).
6. S. Ritsch, C. Beeli, H. U. Nissen, R. Lück, Two different superstructures of the decagonal Al-Co-Ni quasicrystal. *Philos. Mag. A* **71**, 671–685 (1995).
7. S. Ebalard, F. Spaepen, The body-centered-cubic-type icosahedral reciprocal lattice of the Al-Cu-Fe quasi-periodic crystal. *J. Mater. Res.* **4**, 39–43 (1989).
8. A. P. Tsai, J. Q. Guo, E. Abe, H. Takakura, T. J. Sato, A stable binary quasicrystal. *Nature* **408**, 537–538 (2000).
9. H. Takakura, C. P. Gómez, A. Yamamoto, M. De Boissieu, A. P. Tsai, Atomic structure of the binary icosahedral Yb-Cd quasicrystal. *Nat. Mater.* **6**, 58–63 (2007).
10. L. Bindi, P. J. Steinhardt, N. Yao, P. J. Lu, Natural quasicrystals. *Science* **324**, 1306–1309 (2009).
11. L. Bendersky, Quasicrystal with one-dimensional translational symmetry and a tenfold rotation axis. *Phys. Rev. Lett.* **55**, 1461–1463 (1985).
12. W. Steurer, Twenty years of structure research on quasicrystals. Part I. Pentagonal, octagonal, decagonal and dodecagonal quasicrystals. *Z. Kristallogr. Cryst. Mater.* **219**, 391–446 (2004).
13. L. Bindi *et al.*, Natural quasicrystal with decagonal symmetry. *Sci. Rep.* **5**, 9111 (2015).
14. W. Steurer, S. Deloudi, Decagonal quasicrystals – What has been achieved? *C. R. Phys.* **15**, 40–47 (2014).
15. S. Iwami, T. Ishimasa, Dodecagonal quasicrystal in Mn-based quaternary alloys containing Cr, Ni and Si. *Philos. Mag. Lett.* **95**, 229–236 (2015).
16. T. Ishimasa, Dodecagonal quasicrystals still in progress. *Isr. J. Chem.* **51**, 1216–1225 (2011).
17. A. P. Lindsay *et al.*, A15, σ, and a quasicrystal: Access to complex particle packings via bidisperse diblock copolymer blends. *ACS Macro Lett.* **9**, 197–203 (2020).
18. M. W. Schulze *et al.*, Conformational asymmetry and quasicrystal approximants in linear diblock copolymers. *Phys. Rev. Lett.* **118**, 207801 (2017).
19. J. Zhang, F. S. Bates, Dodecagonal quasicrystalline morphology in a poly(styrene-b-isoprene-b-styrene-b-ethylene oxide) tetrablock terpolymer. *J. Am. Chem. Soc.* **134**, 7636–7639 (2012).
20. K. Hayashida, T. Dotera, A. Takano, Y. Matsushita, Polymeric quasicrystal: Mesoscopic quasicrystalline tiling in ABC star polymers. *Phys. Rev. Lett.* **98**, 195502 (2007).
21. A. J. Mueller *et al.*, Quasicrystals and their approximants in a crystalline–amorphous diblock copolymer. *Macromolecules* **54**, 2647–2660 (2021).
22. X. Zeng *et al.*, Supramolecular dendritic liquid quasicrystals. *Nature* **428**, 157–160 (2004).
23. R. Zhang, X. Zeng, G. Ungar, Direct AFM observation of individual micelles, tile decorations and tiling rules of a dodecagonal liquid quasicrystal. *J. Phys. Condens. Matter* **29**, 414001 (2017).
24. K. Yue *et al.*, Geometry induced sequence of nanoscale Frank-Kasper and quasicrystal mesophases in giant surfactants. *Proc. Natl. Acad. Sci. U.S.A.* **113**, 14195–14200 (2016).
25. X. Feng *et al.*, Hierarchical self-organization of AB *n* dendron-like molecules into a supramolecular lattice sequence. *ACS Cent. Sci.* **3**, 860–867 (2017).
26. X. Feng *et al.*, Transition kinetics of self-assembled supramolecular dodecagonal quasicrystal and Frank-Kasper σ phases in ABn dendron-like giant molecules. *ACS Macro Lett.* **8**, 875–881 (2019).
27. A.-P. Tsai, "Back to the future"–An account discovery of stable quasicrystals. *Acc. Chem. Res.* **36**, 31–38 (2003).
28. G. Kurtuldu, K. F. Shamlaye, J. F. Löffler, Metastable quasicrystal-induced nucleation in a bulk glass-forming liquid. *Proc. Natl. Acad. Sci. U.S.A.* **115**, 6123–6128 (2018).
29. A. Hirata *et al.*, Geometric frustration of icosahedron in metallic glasses. *Science* **341**, 376–379 (2013).
30. F. C. Frank, Supercooling of liquids. *Proc. R. Soc. Lond. A Math. Phys. Sci.* **215**, 43–46 (1952).
31. T. M. Gillard, S. Lee, F. S. Bates, Dodecagonal quasicrystalline order in a diblock copolymer melt. *Proc. Natl. Acad. Sci. U.S.A.* **113**, 5167–5172 (2016).
32. Y. Nagaoka, H. Zhu, D. Eggert, O. Chen, Single-component quasicrystalline nanocrystal superlattices through flexible polygon tiling rule. *Science* **362**, 1396–1400 (2018).
33. S. Fischer *et al.*, Colloidal quasicrystals with 12-fold and 18-fold diffraction symmetry. *Proc. Natl. Acad. Sci. U.S.A.* **108**, 1810–1814 (2011).
34. Y. Liu *et al.*, Mesoatom alloys via self-sorting approach of giant molecules blends. *Giant* **4**, 100031 (2020).
35. S. Lee, M. J. Bluemle, F. S. Bates, Discovery of a Frank-Kasper σ phase in sphere-forming block copolymer melts. *Science* **330**, 349–353 (2010).
36. M. Mihalkovic, J. Richmond-Decker, C. L. Henley, MOxborrow, Ab-initio tiling and atomic structure for decagonal ZnMgY quasicrystal. *Philos. Mag.* **94**, 1529–1541 (2014).
37. H. Xie *et al.*, Self-assembly of two unit cells into a nanodomain structure containing five-fold symmetry. *J. Phys. Chem. Lett.* **9**, 4373–4378 (2018).
38. W. Z. Wang, X. Z. Zhou, Z. Q. Yang, Y. Qi, H. Q. Ye, A decagonal quasicrystal with rhombic and hexagonal tiles decorated with icosahedral structural units. *IUCrJ* **7**, 535–541 (2020).
39. D. R. Nelson, B. I. Halperin, Pentagonal and icosahedral order in rapidly cooled metals. *Science* **229**, 233–238 (1985).
40. A. S. Keys, S. C. Glotzer, How do quasicrystals grow? *Phys. Rev. Lett.* **99**, 235503 (2007).
41. K. A. Cavicchi, T. P. Lodge, Self-diffusion and tracer diffusion in sphere-forming block copolymers. *Macromolecules* **36**, 7158–7164 (2003).
42. S. H. Choi, F. S. Bates, T. P. Lodge, Molecular exchange in ordered diblock copolymer micelles. *Macromolecules* **44**, 3594–3604 (2011).
43. M. Impéror-Clerc, A. Jagannathan, P. Kalugin, J.-F. Sadoc, Square-triangle tilings: An infinite playground for soft matter. *Soft Matter* **17**, 9560–9575 (2021).
44. M. Dzugutov, A universal scaling law for atomic diffusion in condensed matter. *Nature* **381**, 137–139 (1996).
45. Z. Jiang, GIXSGUI: A MATLAB toolbox for grazing-incidence X-ray scattering data visualization and reduction, and indexing of buried three-dimensional periodic nanostructured films. *J. Appl. Cryst.* **48**, 917–926 (2015).